TCAD simulations of planar pixel sensors

Abdenour Lounis[1], Mathieu Benoit, Nicoleta Dinu

Laboratoire de l'Accélérateur Linéaire

Université de Paris Sud XI, Centre Scientifique d'Orsay, Bat 200, BP 34, 91898 Orsay cedex, France

E-mail: `lounis@lal.in2p3.fr`

Giovanni Calderini, Marco Bomben, Giovanni Marchiori

Laboratoire de Physique Nucléaire des Hautes Energies, Paris VI, CNRS, 4 place Jussieu - 75252 Paris cedex 05, France

For the ATLAS inner upgrade, Planar Pixel Sensor technology represents one of the options envisaged for the replacement of the innermost layer: the so-called B layer. An in depth simulation program has been carried out to improve the existing geometrical design, not only by minimizing the inactive area at the outer edge but, more important, optimising the signal size after irradiation. We give in this paper all the simulation ingredients used to achieve these improvements. We show how reducing the inactive edge zone, thus increasing the sensitive area, does not have any negative impact on the sensor working conditions. To illustrate these results, electric field profiles in the bulk and lateral depletion voltages are shown as the number of guard rings is reduced for a thinner sensor. Another investigation is focused on simulation models that give a good explanation of the charge multiplication phenomenon, observed experimentally in heavily irradiated sensors.

---

[1] Speaker

1. Introduction

Increasingly performant experimental silicon detector devices are requested for use in high energy experiments which are raising their luminosity to increase their physics potential. In the future, the LHC will be upgraded for High Luminosity LHC (HL-LHC) conditions in two steps, namely phase I for a luminosity of approximately 2.2 x 10^{34} cm^{-2} s^{-1} and phase II which targets a luminosity of 5 x 10^{34} cm^{-2} s^{-1} and ultimatly a total integrated luminosity of 3000 fb^{-1}. To be operational for phase I, at the end of the actual period, the inner pixel layer called B layer will be replaced. A new beam pipe instrumented with a new pixel sensor layer and its associated electronics will be installed at a radius of 33.25 mm from the interaction point [1]. This will raise drastically the radiation levels with respect to the current conditions up to 5 x 10^{15} n$_{eq}$/cm^2. The purpose here is to detail our study of one of the potential detector options: the Planar Pixel Sensor (PPS). The radiation damage on the Planar Pixel Sensors has been carefully studied in several irradiation beam facilities and their behaviour under heavy irradition doses was intensively simulated [2]. Standard n-in-n planar pixel and potential benefits of n-in-p structures are being also investigated and redesigned to be capable or efficiently sustaining the expected harsh irradiation conditions. Advantages and possible drawbacks of the new designs have been scrupulously evaluated to construct the best planar pixel detector for the HL-LHC.

2.Technology Computer Aided Simulation

2.1 Ingredients of the simulation tool

These days physical-based simulation of devices is extremly important. Not only is simulation quicker and cheaper than performing an experiment but it could also give access to a deeper understanding or at least provide insights and/or behaviour of some physics parameters that are hard to obtain by measurements.

The device simulation package used in this work is Silvaco-TCAD [3]. It is a physics based device simulation tool used to study the charge carrier distributions and electric field configurations inside simplified two dimensional models for silicon based devices. One of its major advantages is the possibility to predict the electrical characteristics that are associated with any well defined physical geometrical structure and also bias conditions. So, important known input data must be given at the start: the physical structure to be simulated, all doping profile concentration details, the physical model to be used and the bias conditions for which electrical simulation is to be carried out. Structure specification should be explicitly detailed like adequate meshing, electrode geometrical types, precise oxide thickness and also doping profiles values of implants, interpixel region and guard rings. Material model specification and contact interface are also included in the input data. Various mathematic numerical methods could be chosen to solve a set of fundamental equations. These equations, derived from Maxwell's law are the Poisson equation that relates the electrostatical potential to the charge density and the continuity and transport equations that describe the way that electron and hole density evolve as a result of transport, generation and recombination processes (Shockley Read-

Hall model [4]). Defect centers and traps present in the substrate influence in a significant way the electrical characteristics of the device. Trap centers whose associated energy lies in a forbidden gap, exchange charge with conduction and valence bands through emission and capture of electrons. In addition to ionized donor and acceptor impurities, all mechanisms which add to the space charge, such as fixed interface charges, interface trap states and bulk trap states are taken into account in the Poisson equation and modeled in steady state and transient conditions.

It is important to adequatly model the carrier mobility with respect to the electric field strengh, for high or low field behaviour, bulk region and inversion layers which introduces more specific effects like surface scattering, carrier-carrier scattering and quantum effects.

2.1.1 Optimizing the guard ring region

The simulation, based on a 2D model, is performed on two bulk types that are based on n-in-n and n-in-p structures. Both options are being considered for the future upgrade of the inner ATLAS detector and motivate our choice. The resistivity substrate for   n-in-p and n-in-n structures was simulated with 5 KΩ/cm. The sensor thickness is 285 μm. The initial sensor edge design configuration of 1100 μm overall width includes of a set of 16 guard rings made of implants of width of 10 μm. This region is designed to allow a safe gradual potential drop outside of the sensitive area and has added to it a 300 μm width safety border. One of our targets is to evaluate the effect of diminishing the number of GR, study the effect of their geometrical shape like their relative periodic spacing or width on the planar pixel sensor overall performance. figure 1 illustrates the multiguard ring structures studied in this work.
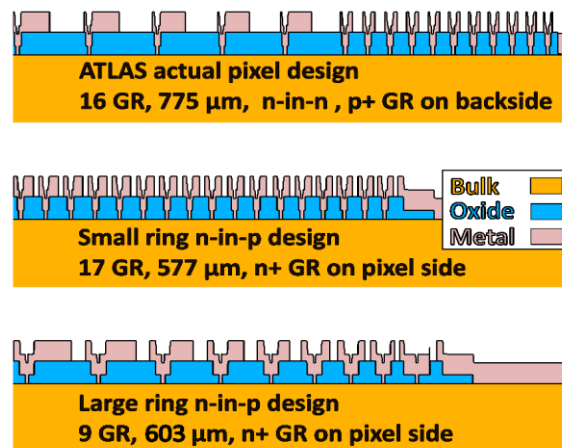

Figure 1: Multiguard ring structures with variable metal overhang
widths. Implants are not depicted.

The electric potential behaviour near the edges after gradual removal of some of the 16 guard rings has been simulated when a reverse biased of 500 V is applied to the sensor. In figure 2, results on the guard rings potential and electric field as a function of their position from the outer edge are illustrated. Since the potential value reaches an almost negligible value when up to 6 guard rings are removed, one can assume that there is no real change to the sensor performance. For the same bias conditions, this result can be verified as shown in the electric field distribution at 0,1 μm under the guard rings versus the distance from the outer edge. One can see that after removing 4 guard rings, the remaining electric field (~40 KV/cm) is extremly weak as compared to the few hundreds of KV/cm required to cause any breakdown situation or generate a noticeable leakage current. The computation of potential at the borders diverges for situations with more than 6 rings removed (breakdown) and are note shown .
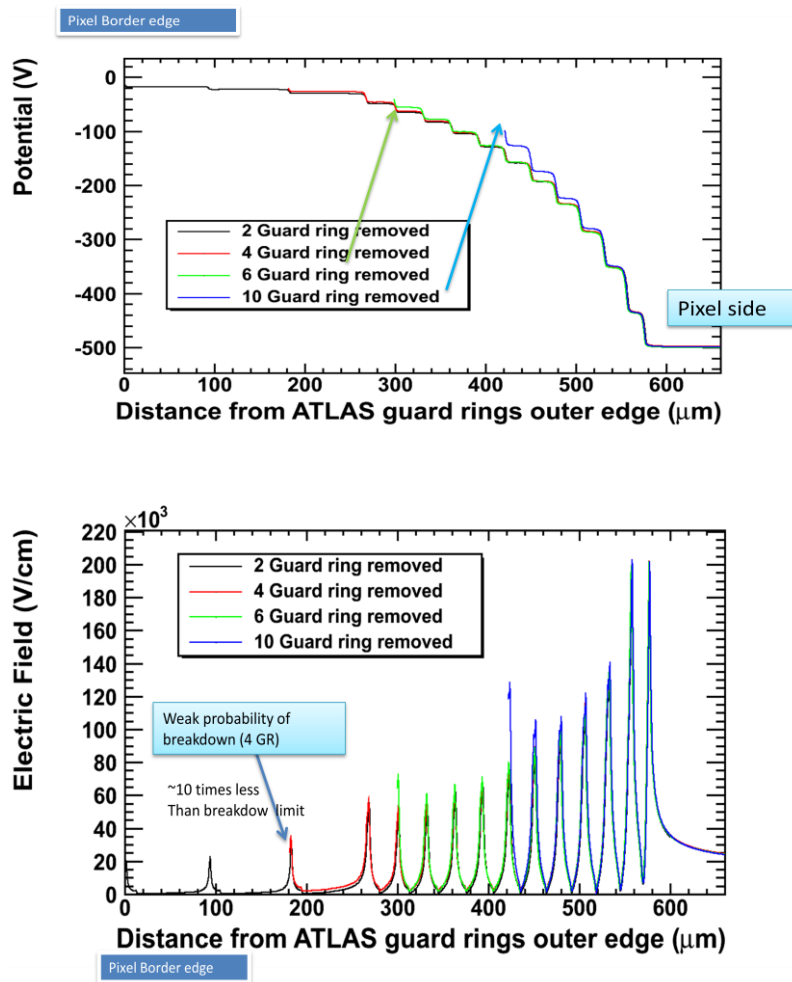

Figure 2 : Guard Ring Potential Voltage (Upper plot) and Electric field (lower plot) distributions as a function of distance from outer edge.

To validate our TCAD simulation procedure, the potential on each guard ring has been measured using a probe station in a clean room and compared to the simulation results. The next

figure summarizes the results obtained and shows a rather good consistency between our simulation and the experimental results for various sensor bias voltages. These make us confident in the correctness of the simulation code and the procedure used in this work.
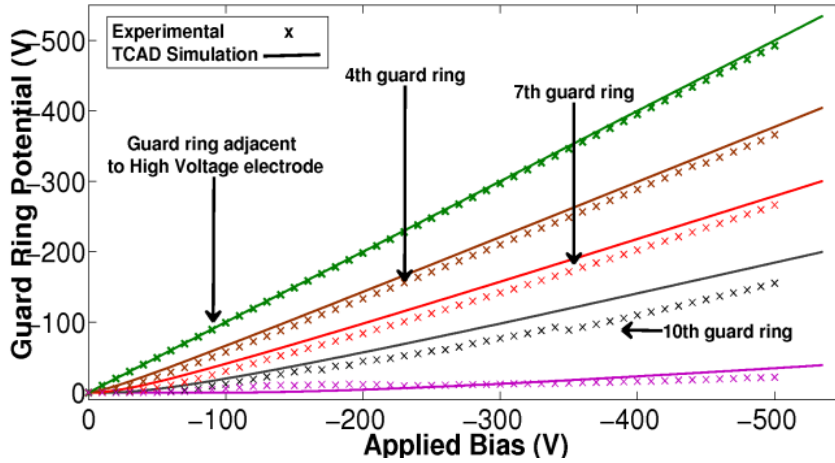

Figure 3 : Comparison of the TCAD results to guard ring potential voltage measurements as a function of the applied bias voltage

2.1.2 Dead zone width optimization

The region Δ between the most outer guard ring and the sensor border had initially a 300 μm width. This insensitive area is used as a safety zone to protect the active area from possible cristal damages or micro-cracks, drop in breakage resistance or stress created at the ends during wafer dicing. Reducing Δ to 100 μm, has shown no influence on the guard ring behaviour as can be seen in figure 4 for the electron concentration distribution as a function of the distance from the edge. One can clearly see that the lateral depletion boundary area stays sufficiently far away from the borders of the sensor and no malfunction is thus forseen if we decrease the border size region to 100 μm which represents without any penality, a gain of the sensitive area.
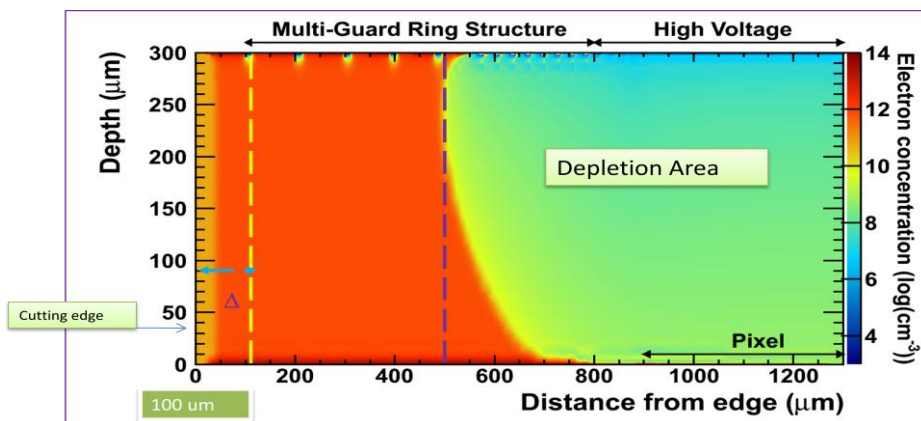

Figure 4 : Electron concentration ($\log(cm^{-3})$) as a function of the distance from the edge

2.1.3 Influence of guard ring geometrical structure

The three different guard ring structures studied here are shown in figure 1. Table 1 summarizes their characteristics.

Name	Sensor type	Number of GR	Total size GR width (μm)	GR on Front (pixel)/Back side
ATLAS GR	n-in-n	16	775	p^+ on Back
SMALL GR	n-in-p	17	577	n^+ on Front
LARGE GR	n-in-p	9	603	n^+ on Front

Table 1: sensor type description

A simulation has been carried out on the three models to evaluate, for various bias voltages, how the geometrical shape and positions of these various guard rings designs might affect the sensor behaviour. In particular, the simulation has been performed at low (50 V), intermediate (100-200 V) and high (300-400 V) bias voltages for the three designs. Results of the majority carrier concentration profile at half depth, for different designs and bias voltages as a function of the distance from the cutting edge are shown in figure 5. No influence of the guard ring design or geometry is seen on the lateral depletion, which is defined as the distance where the concentration falls abruptly. For low voltage at 50 V, one can notice different profile shapes which are all far away, anyway, from the borders. For this particular situation, the sensor is still under-depleted, so has not yet reached its optimal regime. This result allowed us to conclude that geometrical structure of the guard ring designs has no significant influence on the lateral depletion.
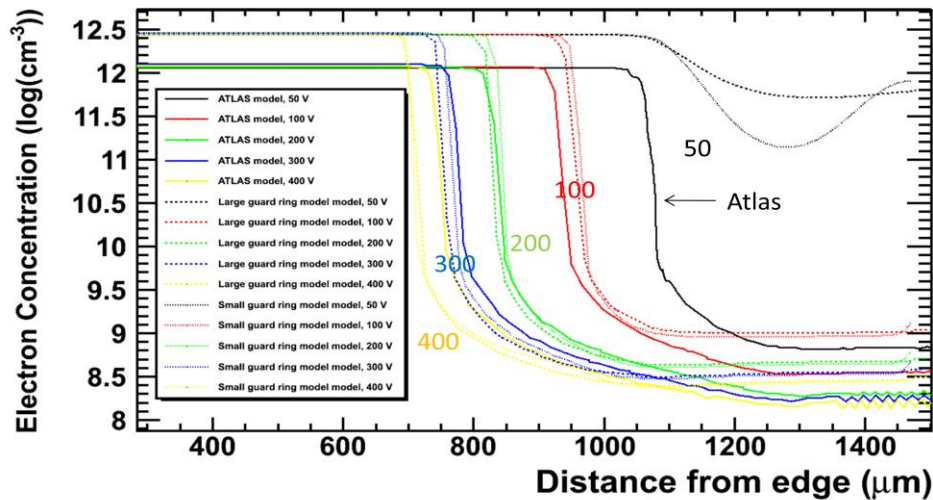

Figure 5: Lateral depletion and electron concentration for ATLAS, SMALL and LARGE ring strutures

2.1.4 Bulk thickness influence

An important issue for modern tracking in high energy experiments is the material budget of your detector as sensors with a short radiation length improve the tracking performance. Small thickness reduces multiple scattering in the detector and diminishes the carrier trapping probability in the bulk. So, the reduction of silicon sensor thickness has been studied in this simulation. Moreover, silicon sensor operation with very high electric field would raise charge yield in high irradiation conditions where charge amplification could occur. Capacitance evaluation for different sensor thicknesses has been simulated in a previous work (see [5]) and is necessary to evaluate the performance of the sensors in terms of charge over noise and threshold.

From figure 6, one can see that for 150 V bias voltage, the electric field distribution at 1 μm under the pixel does not change for the three thickness sizes of 150, 200 and 250 μm.

No modifications for the peak electric field are observed at the guard ring level for thick or thin sensors. The explanation is that although the mean electric field is higher for thinner sensors, no lateral geometrical modification is introduced and the lateral voltage remains unchanged.
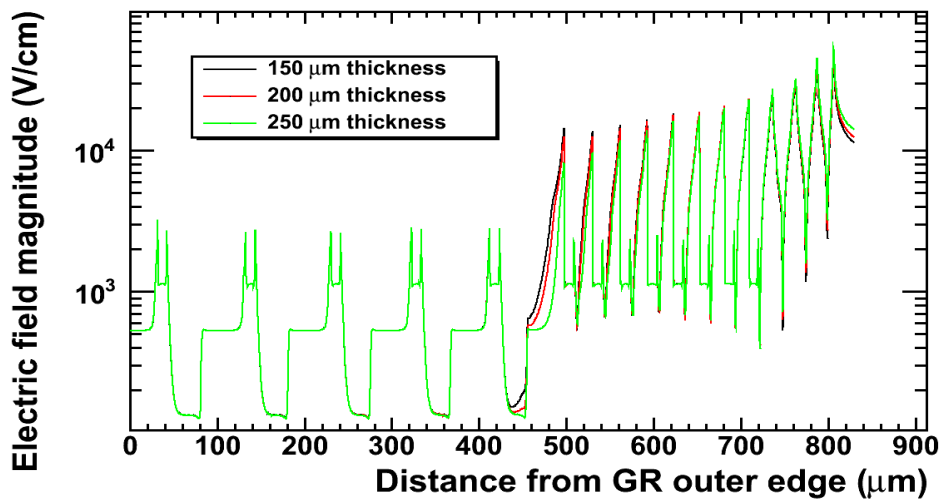

Figure 6: Simulation of electric field distribution at 1 micron under guard rings for three thicknesses

We can conclude from this study that for the same bias voltage, reduction of the sensor thickness does not modify the guard ring functionality. This is an argument in favor thin sensors compared to thick one, as they could be fully depleted at lower voltage. In high irradiation conditions, thin sensors have also the advantage to allow smaller carrier trapping inside the bulk due to short travel paths of electron and holes.

2.1.5 The slim edge guard ring structure

      One new idea to reduce further the inactive area of n-in-n sensors is to shift inwards the guard ring structure on the backside of the sensor. This geometrical structure is shown in figure 7. TCAD simulation has been carried out on an actual ATLAS n-in-n model for which guard rings were shifted successively under the pixel region by 100, 200 and 400 μm. In the simulation a bias voltage of 100 V was used for a 300 μm sensor thickness. As electron carriers could travel away from from the pixel region, one could expect some charge loss in the outer pixel, as shown in the potential voltage distribution versus depth of figure 8-a). However it will only have a minor effect for an unirradiated sensor performance, as the amount of charge collected is anyway generally over the electronic threshold. In case the sensor is irradiated to 1x 10^{15} n_{eq}/cm^2 , as shown in figure 8-b), space charge sign inversion (SCSI) occurs and makes the sensor depletion starting from the pixel region rather than from the backside region as it is the case for non-irradiated actual ATLAS n-in-n sensors.
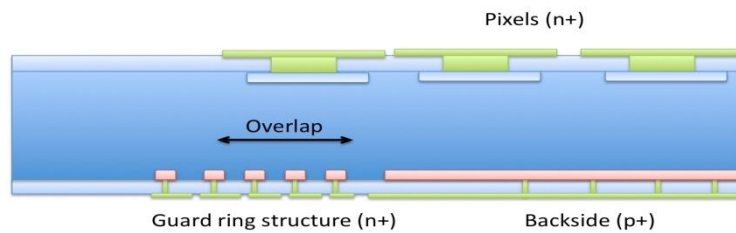

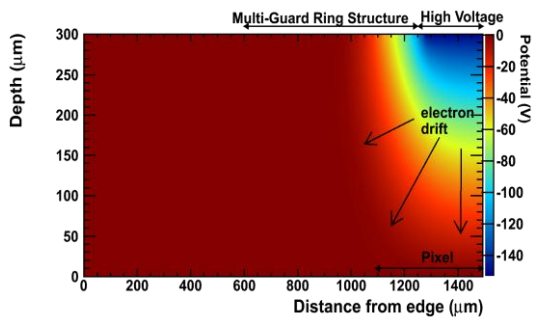Figure 7: Slim edge : n+ on n bulk, multi-guard ring structure.

Figure 8-a) Potential distribution inside the   Figure 8-b) After irradiation and
unirradiated Sensor bulk: electric field   SCSI, no field distortion appears and
distorsion lead to charge loss in the pixel   all electron carriers are collected.

      No lateral depletion appears   near the pixel implant thus   the full charge will be collected at the pixel electrode. The conclusion one can draw from this simulation is that slim edge design turns out to be a good solution to improve the active area in n-in-n sensor, especially after heavy irradiation.

3. Simulation of heavily irradiated structures

3.1 Electric field profile

The charge collection efficiency of microstrip sensors has been studied by the RD50 collaboration [6]. Results have shown that at fluences greater than 2x 10^{16} n_{eq}/cm^2, planar sensors can yield a signal equal or even greater than before irradiation [7,8]. To enable this charge amplification effect, operation at high voltages over 1000 V are necessary. Thanks to TCAD simulation, we have investigated the charge amplification phenomenon in a simple one dimensional diode geometry. Electric field profiles at high bias voltages for unirradiated and irradiated thick and thin diodes have been computed and results are shown respectively in figure 9-a) and 9-b). One can note that for irradiated sensors, electric field greater than 90 KV/cm occurs in the bulk, suggesting a potential detrapping process of carriers and possible charge multiplication. For non irradiated diodes, one can notice that electric field pinching would certainly induce a hard breakdown which makes such devices not usable at these high bias voltage ranges. The impact ionization model used in our simulation occurs at high electric field in a space charge region with a sufficiently high reverse bias. The physics mechanism is the following. If the electric field, accelerating the free carriers, is sufficiently high and the distance between carrier collisions is short enough, it could accelerate free carriers to high velocity. Free carriers acquire sufficient energy before colliding with crystal atoms. Thus more carriers are generated and if the generation rate exceeds a given level, avalanche breakdown occurs.
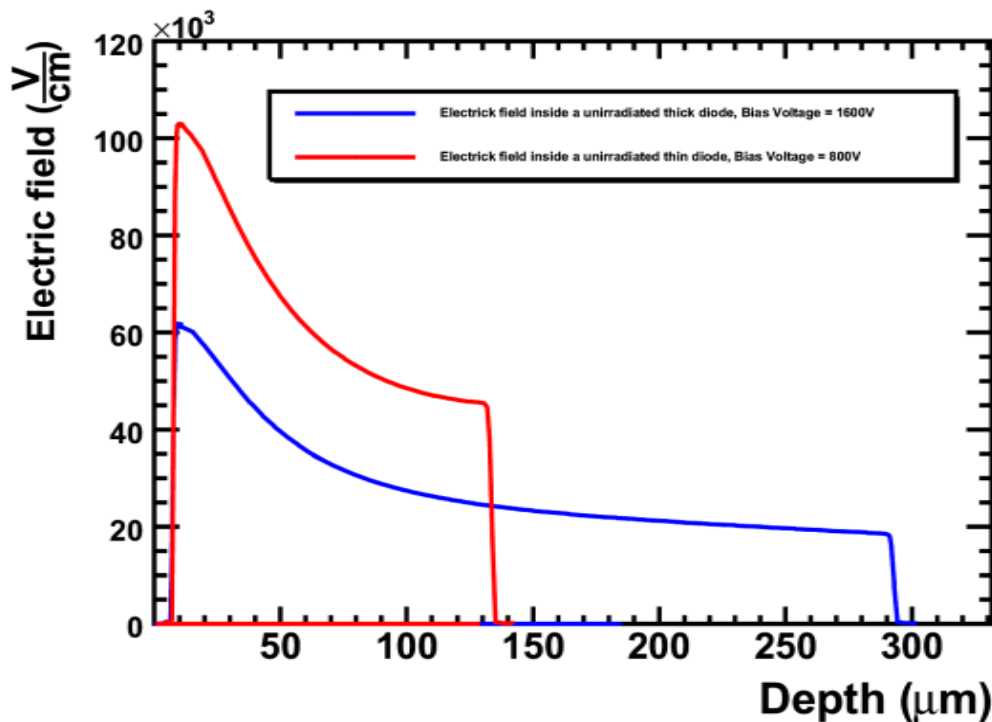

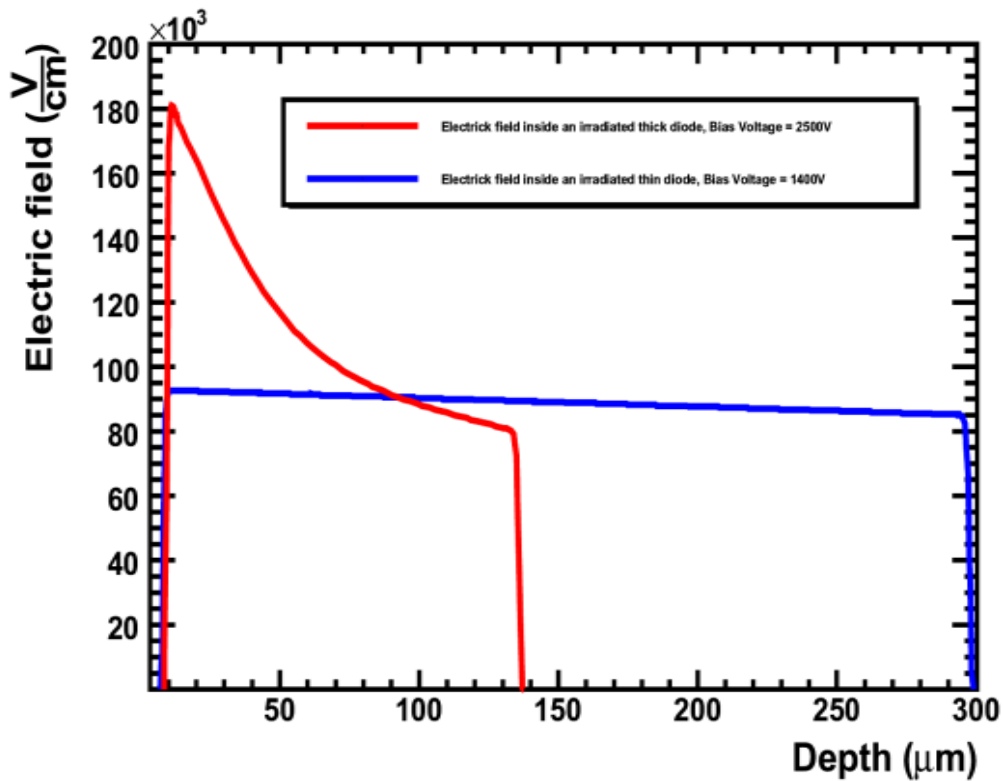Figure 9-a Electric field profiles for unirradiated for thick (in blue) and thin (in red) diode

9

Figure 9-b Electric field profiles irradiated thick (in blue) and thin (in red) diode at a fluence of 2 x 10^{16} n_{eq}/cm^2

3.1 Charge collection efficiency

Transcient simulation has been also carried out on the sensor device. A 2ns triangular 1060 nm laser pulse was sent perpendicular to the device surface. Ionization charges are deposited uniformely in the bulk depth. A transcient simulation over 40 ns at various bias voltages has then been computed. At high electric field, tunneling of electrons from the valence band to conduction band through trap or defects states has an important effect on the current emission. Trap assisted tunneling is included in the simulation in terms of enhancement of the trap lifetime factor which is described in the model as the effect of phonon assisted tunneling on the emission of electrons and holes from a trap. The quenching mechanism in heavily irradiated sensors has as a consequence the increase of trapping time avoiding breakdown in the multiplication regime. The signal obtained by the simulation is integrated and pedestal substracted to end up with the net charge collection. Charge collection efficiency is obtained by dividing the net charge collected by the total charge deposited in the bulk. One can deduce from the figure 10-a, that the multiplication effect can be seen only at very high voltage much beyond the breakdown voltage in unirradiated sensors, so in unrealistic conditions. However for heavily irradiated sensors seen in figure 10-b, we do see an increase of charge collection efficiency greater than 1 over 1000 V bias voltage at the condition that two mechanisms namely impact ionization and trap to band tunneling are both turned on in the simulation model.
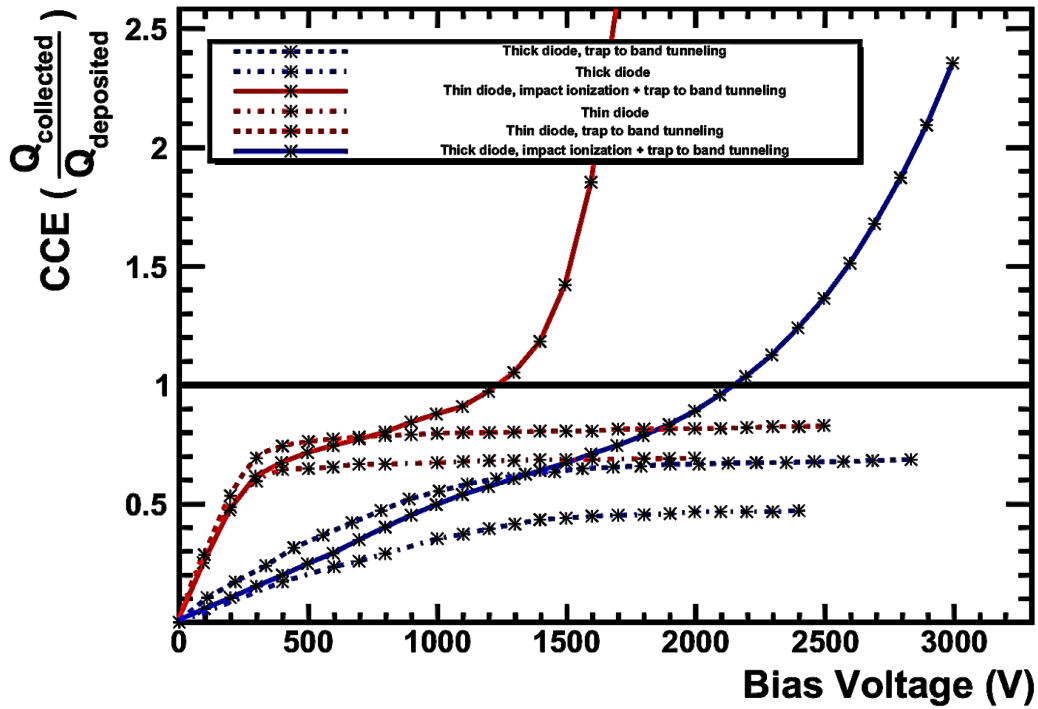
Figure 10-a: Charge collection efficiency as a function of bias voltage for an non-irradiated thick and thin sensor
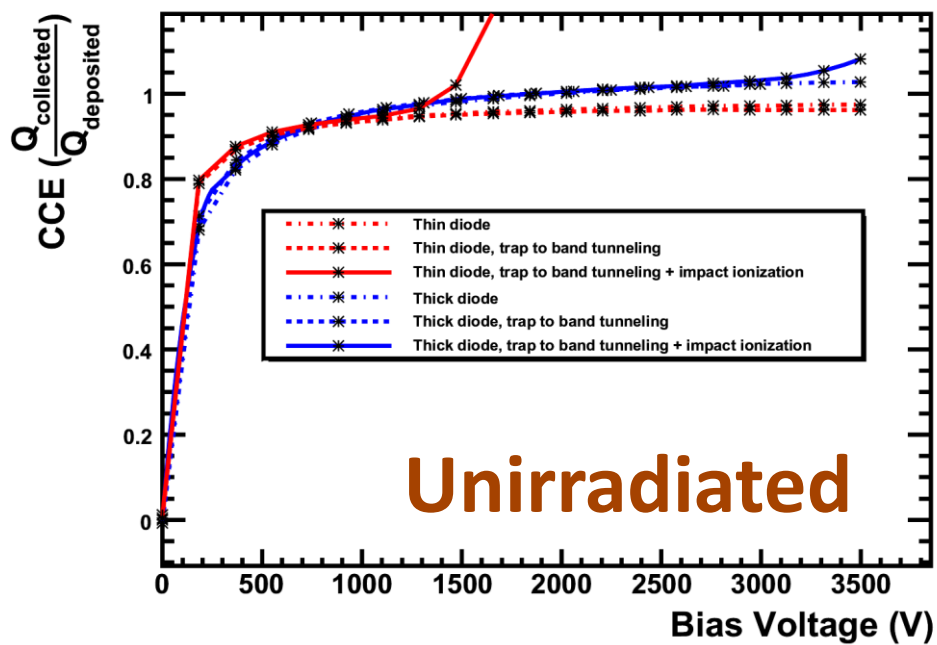

Figure 10-b: Charge collection efficiency as a function of bias voltage for a thick and thin sensor at $2x10^{16}$ n_{eq}/cm^2

4. Summary

TCAD simulation of planar pixel sensors for IBL ATLAS project has been intensively carried out [9,10,11,12] and is presented here. The simulation carried on the geometrical design has shown that a substancial reduction of the insensitive sensor edge area is possible without any drawback by firstly removing 6 guard rings and secondly lowering to 100 μm the width the outer dead edge region; this will not bring any deterioration to the performance of the planar pixel sensors. Various guard ring configurations (size, spacing and interspace widths) labelled small, large and ATLAS were tried and haven't shown any effect on the sensor behaviour. The study on bulk thickness reduction has shown no influence on the guard rings behaviour. Finally, charge collection amplification at high bias voltage in heavily irradiated sensors could be well interpreted by the contribution of two physics mechanisms added simultaneously namely impact ionization and trap to band tunneling in the semiconductor medium.

5. Aknowlegments

References

[1] ATLAS Insertable B layer, CERN-LHCC 2010-013, ATLAS TDR **19** , 15/09/2010

[2] M. Benoit, PhD dissertation, Université de Paris XI, June 10th, 2011,Ref. LAL-11-118, unpublished.

[3] Silvaco International inc, 4701 Patrick Henry Driven bldg 1, Santa Clara CA 95054, *ATLAS User's manual, Device Simulation Software, June 2008. V 5.14.0.R 77*

[4] W.Shockley, W.T Read, Phys. Rev. 87 (1952)835

[5] G. Calderini, M. Benoit, N. Dinu, A. Lounis and G. Marchiori, Nuclear Instrument and Methods in Physics Research A 636 (2011)537-541.

[6] CERN-RD50 Collaboration, http://rd50.web.cern.ch/rd50/

[7] G. Casse and al., Nuclear Instrument and Methods in Physics Research A636 (2011)S56-S61

[8] M. Mikuz and al, Nuclear Instrument and Methods in Physics Research A636 (2011)S50-S55

[9] M. Benoit, A. Lounis, , D. Martinot, G. Calderini, , N. Dinu, ATL- UPGRADE-INT-2010-02, CERN, Geneva, Oct 2010, 84

[10] M. Benoit, A. Lounis and N. Dinu, Journal of Instruments, vol 4, no 03, (2009) P03025

[11] M. Benoit, A. Lounis and N. Dinu, Nuclear Science IEEE Transactions on, Vol 56 (2009) 3236-3243

[12] A. Lounis, , D. Martinot, G. Calderini, M. Benoit , N. Dinu, ATL-COM-UPGRADE-2009-013,
      CERN, Geneva, Oct 2009, 84